



Observed Decadal Changes in Downward Wave Coupling between the Stratosphere and Troposphere in the Southern Hemisphere

NILI HARNIK

Department of Geophysics and Planetary Sciences, Tel Aviv University, Tel Aviv, Israel

JUDITH PERLWITZ

Cooperative Institute for Research in Environmental Sciences, University of Colorado, and NOAA/Earth System Research Laboratory/Physical Sciences Division, Boulder, Colorado

TIFFANY A. SHAW

Lamont-Doherty Earth Observatory, and Department of Applied Physics and Applied Mathematics, Columbia University, New York, New York

(Manuscript received 7 October 2010, in final form 15 February 2011)

ABSTRACT

Downward wave coupling dominates the intraseasonal dynamical coupling between the stratosphere and troposphere in the Southern Hemisphere. The coupling occurs during late winter and spring when the stratospheric basic state forms a well-defined meridional waveguide, which is bounded above by a reflecting surface. This basic-state configuration is favorable for planetary wave reflection and guides the reflected waves back down to the troposphere, where they impact wave structures. In this study decadal changes in downward wave coupling are analyzed using the Modern Era Retrospective-Analysis for Research and Applications (MERRA) dataset.

A cross-spectral correlation analysis, applied to geopotential height fields, and a wave geometry diagnostic, applied to zonal-mean zonal wind and temperature data, are used to understand decadal changes in planetary wave propagation. It is found that downward wave 1 coupling from September to December has increased over the last three decades, owing to significant increases at the beginning and end of this 4-month period. The increased downward wave coupling is caused by both an earlier onset of the vertically bounded meridional waveguide configuration and a persistence of this configuration into December. The latter is associated with the observed delay in vortex breakup. The results point to an additional dynamical mechanism whereby the stratosphere has influenced the tropospheric climate in the Southern Hemisphere.

1. Introduction

During the last three decades, the extratropical Southern Hemisphere has undergone significant climate changes. These changes are most apparent during spring and early summer and include a cooling of the polar stratosphere, a delay of the breakup of the polar vortex, and an increase in the strength of the tropospheric westerlies together with surface cooling over the Antarctic

interior and a warming over the Antarctic Peninsula (e.g., Waugh et al. 1999; Thompson and Solomon 2002). These changes have been mostly attributed to stratospheric polar ozone depletion (e.g., Gillett and Thompson 2003), which affects the troposphere via annular mode dynamics [see Son et al. (2010) for an overview of possible mechanisms]. More recently, it has been noted that there is a strong nonzonal component to Southern Hemisphere climate trends (e.g., Johanson and Fu 2007), which are associated with significant changes in planetary wave structure from the troposphere to the stratosphere (Neff et al. 2008; Lin et al. 2009; Hu and Fu 2009). Hu and Fu (2009) attributed the stratospheric changes in planetary wave structure to an increase in

Corresponding author address: Nili Harnik, Department of Geophysics and Planetary Sciences, Tel Aviv University, Tel Aviv 69978, Israel.
E-mail: harnik@tau.ac.il

upward planetary wave activity flux caused by changes in sea surface temperature (SST); however, the nature of decadal changes in wave dynamics are still not well understood.

It is well known that wave activity propagation from the troposphere to the stratosphere in the Southern Hemisphere maximizes during austral spring (Randel 1988). When the upward propagating waves reach the stratosphere, they either dissipate and initiate zonal-mean stratosphere–troposphere coupling or they are reflected downward toward the troposphere, which results in downward wave coupling (Perlwitz and Harnik 2004; Harnik 2009). Recently, Shaw et al. (2010) showed that climatological downward wave coupling is stronger than zonal-mean coupling on the intraseasonal time scale in the Southern Hemisphere, particularly during austral spring. They found significant downward wave coupling beginning in September–October, peaking in October–November, and decaying toward the breakup of the vortex in November–December. The strong wave coupling was attributed to the formation of a bounded wave geometry involving a high-latitude meridional waveguide in the lower stratosphere, bounded above by a vertical reflecting surface, which occurs as part of the seasonal cycle. The meridional waveguide focuses the upward-propagating waves toward the vertical reflecting surface in the stratosphere and upon reflection, back down into the troposphere.

The goal of this paper is to investigate the impact of the observed changes in the extratropical Southern Hemisphere on downward wave coupling between the stratosphere and troposphere. We show that downward wave coupling from September to December has increased significantly over the last three decades because of changes in the wave geometry. The datasets and the analysis approach are described in section 2, the results are presented in section 3, and the findings are summarized in section 4.

2. Data and analysis approach

The reanalysis data used in this study are the daily three-dimensional geopotential heights, and zonal-mean zonal wind and temperature fields from the Modern Era Retrospective-Analysis for Research and Applications (MERRA) reanalysis dataset (Rienecker et al. 2011; Schubert et al. 2008) covering the period from 1979 to 2009. Shaw et al. (2010) used the 40-yr European Centre for Medium-Range Weather Forecasts (ECMWF) Re-Analysis (ERA-40) dataset in their study. They noted that ERA-40 and MERRA were consistent in their climatologies of downward wave coupling in the Southern Hemisphere.

Downward wave coupling is analyzed using the diagnostics of Shaw et al. (2010). A cross-spectral correlation technique (Randel 1987) is used to isolate upward and downward propagating planetary wave signals. The diagnostic considers two geopotential height Fourier coefficients of wavenumber k at two different latitudes and heights and determines their coherence correlation and phase as a function of time lag. Statistically significant cross correlations for time lags when the stratosphere leads the troposphere indicate downward wave coupling. We focus on zonal wave 1 and use a reference latitude band from 45° to 80°S and a reference level at 500 hPa. Further details can be found in Shaw et al. (2010). To examine decadal variations, we apply the diagnostic to 10-yr periods. To examine seasonal variations, we use reference time series spanning the following four periods: 1 September–16 December, 1 September–16 October, 1 October–15 November, and 1 November–16 December. Considering the autocorrelation of tropospheric and stratospheric wave 1 fields (for approach see Lau and Chan 1983), decadal stratospheric correlation coefficients greater than 0.18 and 0.2 are significant at the 99% level for the 3.5- and 1.5-month correlations, respectively.

The wave geometry diagnostic of Harnik and Lindzen (2001) is used to relate the downward wave coupling to the basic state (i.e., to the zonal-mean zonal wind and temperature). The diagnostic separates the more commonly used index of refraction into vertical and meridional wavenumber contributions. As for the squared index of refraction, waves propagate in the vertical direction when $m^2 > 0$ (m is real), are evanescent when $m^2 < 0$ (m is imaginary), and are reflected when they reach a surface where $m^2 = 0$. Similarly, wave propagation in the meridional direction depends on the sign of l^2 . The wave geometry diagnostic is used to determine whether the basic state allows wave propagation in the vertical and meridional directions. The wavenumber results presented here are based on 5-day running means of zonal-mean zonal wind and temperature data. The MERRA data were subsampled at every second latitude (2.5° resolution) to facilitate the handling of the data. The results were very similar to those when the full (1.25° resolution) data were used. The wavenumbers were averaged using their squared values as follows: $\langle m \rangle = \sqrt{|\langle m^2 \rangle| \text{sign}(\langle m^2 \rangle)}$, where $\langle \cdot \rangle$ denotes an average and $|\cdot|$ denotes the absolute value. Further details can be found in Shaw et al. (2010) and Harnik and Lindzen (2001).

3. Results

We begin by examining the cross correlations during the following three decades: 1979–88; 1989–98; and

1999–2009 (the anomalous stratospheric sudden warming year 2002 is excluded from the last decade¹). Figure 1 shows the wave 1 cross correlations with a reference latitude band from 45° to 80°S at 500 hPa for vertical levels from 500 to 1 hPa and for time lags between -10 and 10. As mentioned in section 2, we display the periods of September–December and the subperiods of September–October, October–November, and November–December (from top to bottom, respectively). Only significant correlation values are contoured. All plots show a peak at zero lag in the troposphere and a peak at positive lags in the stratosphere, indicating upward wave propagation. Most plots (except for the second and fourth rows, first column) also show significant correlation peaks for negative lags, indicating downward wave correlations. The shading in the second and third decades indicates regions where the differences in correlations relative to the first decade are significant at the 90%, 95%, and 99% levels. Statistical significance is quantified using a Monte Carlo test—by first selecting two random 10-yr subsets of the full 31-yr dataset, then calculating the time-lagged correlation for each subset, and finally subtracting the two to obtain the difference in correlation as a function of time lag and height. This process is repeated 500 times, for each of the subseasonal reference periods, to determine the significance levels.

Following Shaw et al. (2010), we begin by considering the entire reflective season (September–December, top row of Fig. 1). We see from the shaded regions that the correlations for negative lags increased significantly during the second and third decades, implying that downward wave coupling has increased with time over the past 30 years. The significant increases in the stratosphere occur at lags of -3 days (shading between 20 and 1 hPa, middle and right columns of top row). There are also increases in the tropospheric correlations at around ± 7 (shading between 500 and 200 hPa, middle and right columns of top row).

The 1.5-month correlations (second through fourth rows) show that during 1979–88, downward correlations were only significant during October–November (there are no significant downward correlations during September–October or November–December, as can be seen by the lack of a significant correlation peak at negative time lags). During the later two decades, conversely, the correlations became significant during

September–October and lasted into November–December. The shadings indicate significant increases in downward correlations during September–October (second row) and November–December (bottom row) but not during October–November (third row). This suggests that the increase in downward correlations during September–December mostly occurred at the beginning and end of the reflective season but not during its peak. For the November–December period, we also see significant increases in the stratospheric positive time-lag correlations, which are suggestive of increased upward propagation. We will show later on that this is consistent with a tendency of the vortex to last longer during the later two decades. During September–October, we also see significant changes in tropospheric correlations (middle column, second row) for both negative and positive time lags, indicating a possible change in tropospheric wave source. The appearance of symmetric peaks at positive and negative time lags is suggestive of traveling waves.

Next we examine the decadal changes in the basic state using the wave geometry diagnostic. As mentioned earlier, the wave geometry assesses the wave propagation characteristics of the basic state. The ability of waves to propagate in the vertical and meridional directions is determined by looking at the vertical (m) and meridional (l) wavenumbers separately. Figure 2 shows decadal averages of the mean vertical wavenumber for 1 September–16 October. The shading indicates regions where waves cannot propagate in the vertical direction (wave evanescence regions), and the evanescent region boundary (thick black contours), is called a reflecting surface. In particular, the reflecting surface in the upper-stratosphere high latitudes will reflect upward-propagating waves back downward. The decadal panels suggest that the reflecting surface moved down and widened over the last three decades with relatively little change in the vertical wavenumber at lower levels. Figure 2d shows the yearly time series of the squared September–16 October mean vertical wavenumber averaged from 50° to 70°S and from 5 to 1 hPa (representing the vertical boundary of the meridional waveguide). During this period, a vertical reflecting surface forms in this region as part of the climatological seasonal cycle (Shaw et al. 2010), so the area-averaged m^2 changes from being positive (real m) to negative (imaginary m). A more negative m^2 index in Fig. 2d thus means the reflecting surface formed earlier in the season (this was verified by looking at the daily seasonal cycles of the three decades). Consistent with the decadal panels, there is a clear negative trend (significant at the 98.7% level, based on a single-sided t test, with $|t| = 2.35$), suggesting that the upper stratosphere between 50° and

¹ None of the results change when we include 2002 (as can be seen from Table 1). Nonetheless, we exclude 2002 because a sudden warming indicates strong wave absorption, while the formation of a reflecting surface results in further wave reflection, which inhibits further wave absorption. Indeed, the two processes seem to be exclusive (Perlwitz and Harnik 2004).

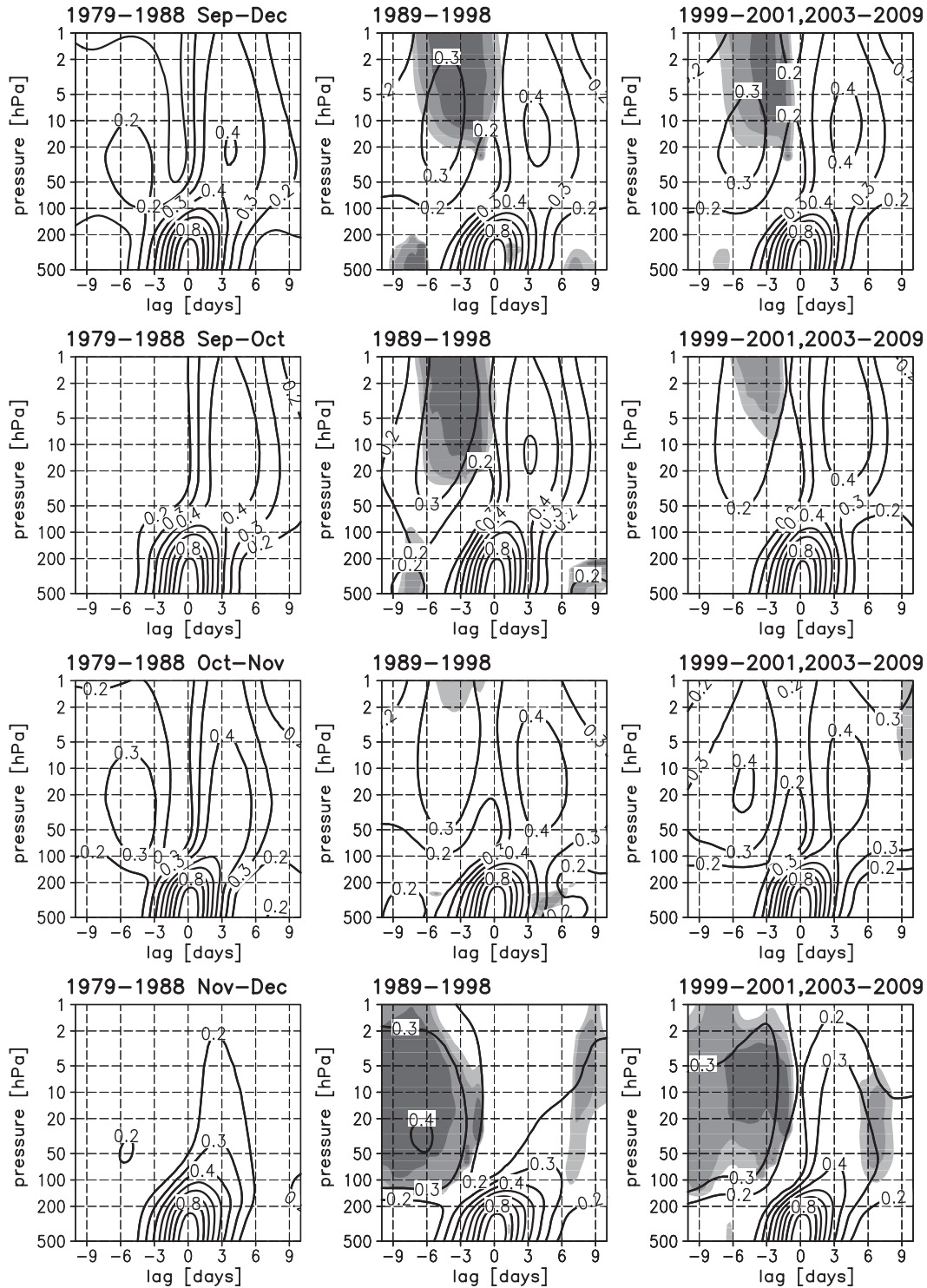


FIG. 1. Correlation coherence for wave 1 averaged from 45° to 80°S at 500 hPa with vertical levels between 500 and 1 hPa during (first row) September–December, (second row) September–October, (third row) October–November, and (bottom) November–December, for three decades: (left) 1979–88, (middle) 1989–98, and (right) 1999–2009, excluding the sudden warming year of 2002. Since the correlations are relative to the 500-hPa level, negative lags mean the stratosphere leads. Light, intermediate, and dark shadings indicate regions in which the differences in correlation from the first decade are significant at the 90%, 95%, and 99% levels, respectively.

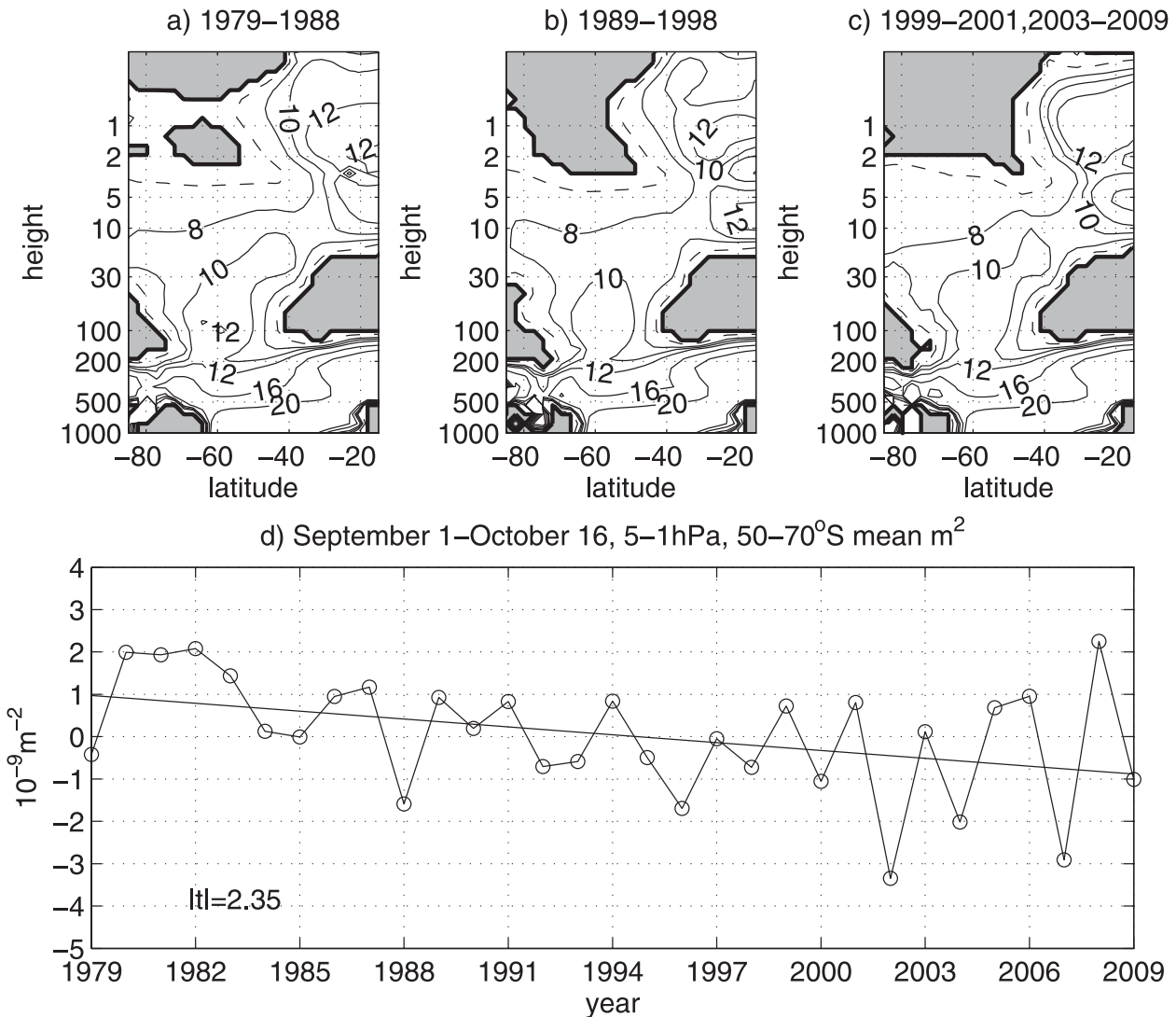


FIG. 2. Decadal mean vertical wavenumbers for 1 Sep–16 Oct for (a) 1979–88, (b) 1989–99, and (c) 1999–2009, excluding 2002. Evanescent regions (negative m^2) are shaded. Contour values, in units of 10^{-5} m^{-1} , are 0 (thick), 4 (dashed), and 8, 10, 12, 16, and 20 (solid). (d) Yearly values and linear best-fit regression (straight line) of the 1 Sep–16 Oct mean vertical wavenumber squared, averaged over 5–1 hPa and $50^\circ\text{--}70^\circ\text{S}$ (units of 10^{-9} m^{-2}).

70°S has become more evanescent for vertical wave propagation over the last three decades. We note, however, that the record is not long enough to establish a long-term trend. In fact, much of the trend is due to the first five years or so having relatively large values (the trend starting from 1985 is only significant at the 84% level).

To better establish the robustness of these changes, we further examine the sources of the trend in m^2 . The sum of the vertical and appropriately scaled meridional wavenumbers squared is roughly the index of refraction squared (n_{ref}^2 ; e.g., Harnik and Lindzen 2001; Shaw et al. 2010). In Cartesian coordinates, this takes the form

$$n_{\text{ref}}^2 \equiv \frac{N^2}{f^2} \left[\frac{\bar{q}_y}{U} - k^2 + F(\rho, N^2) \right] = m^2 + \frac{N^2}{f^2} l^2, \quad (1)$$

where U and \bar{q}_y , and N^2 are the basic-state zonal-mean zonal wind, the meridional gradient of potential vorticity, and the Brunt–Väisälä frequency, respectively. Here k is the zonal wavenumber, and we assumed a stationary wave (zero zonal phase speed). $F(\rho, N^2)$ is a function of density ρ and N^2 . It is not a dominant term, and its exact form can be found in Harnik and Lindzen (2001; see also Shaw et al. 2010). The q_y term, which is dominant in shaping n_{ref}^2 , depends on the zonal-mean wind and N^2 as follows:

TABLE 1. Statistical features of the 1 Sep–16 Oct 50°–70°N means of the 5–1-hPa mean m^2 (shown in Fig. 2d) and the 10–1-hPa means of U_{zz} (Fig. 3b), \bar{q}_y , N^2 (Fig. 3a), U_z , and U . Shown are the detrended correlation coefficients with the m^2 index and the absolute t value $|t|$ of the trend slope using all years and excluding the sudden warming year 2002. Correlations significant at the 99% level based on a two-sided student t test, assuming each year is independent, are in bold. Linear regression $|t|$ values significant at the 95% and 99% levels, based on a single-sided test, are in italic and bold, respectively.

	Correlation with $\langle m^2 \rangle$	$ t $ value for linear trend slopes	
		Without 2002	All years
$\langle m^2 \rangle$	1.0	2.24	2.35
$\langle U_{zz} \rangle$	-0.73	0.63	0.02
$\langle q_y \rangle$	0.62	1.90	2.05
$\langle N^2 \rangle$	0.60	3.51	3.55
$\langle U_z \rangle$	0.25	2.56	2.01
$\langle U \rangle$	0.66	1.05	1.40

$$\bar{q}_y = \beta - U_{yy} + \frac{f^2}{N^2} \frac{U_z}{h} - \frac{f^2}{N^2} U_{zz} + f^2 U_z \frac{N_z^2}{(N^2)^2}, \quad (2)$$

where h is the density-scale height. Plugging this expression for \bar{q}_y into Eq. (1) and assuming the terms involving vertical derivatives of the zonal-mean wind affect m^2 (while the terms involving the meridional derivatives of U affect \bar{q}_y) and that the density-scale height is much smaller than the temperature scale height (neglect the last relative to the third term on the right-hand side), we get the following approximate relation for m^2 :

$$m^2 \approx \frac{N^2}{f^2} \beta + \frac{U_z}{h} - U_{zz}. \quad (3)$$

Thus, we expect m^2 to be positively correlated with N^2 and U_z and negatively correlated with U_{zz} . We calculate the 50°–70°S and 10–1 hPa 1 September–16 October mean values of U_z , U_{zz} , \bar{q}_y , N^2 , and U to obtain the yearly time series. The winds U_z and U_{zz} were calculated using a standard finite differencing in height for grid points at 1 hPa, 10 hPa, and the height level in between. Calculating the finer vertical resolution version of these quantities did not change the results. Also, the vertical and meridional averaging ranges were chosen to maximize correlations with m^2 ; however, taking slightly different averaging ranges did not change the qualitative results.

Table 1 shows the correlations of these quantities with the m^2 index shown in Fig. 2d. We see that U_{zz} is negatively correlated and N^2 is positively correlated with m^2 , suggesting both fields contribute to the interannual variability in the vertical wavenumber in this region and period. The correlation of U_z with m^2 , however, is small. This Southern Hemisphere result differs from

the findings of Perlwitz and Harnik (2003) for the Northern Hemisphere, in that vertical wave reflection occurs during winters when the vertical shear of the zonal-mean wind (U_z) becomes negative in the upper stratosphere. The reason for this difference is most likely because in the Northern Hemisphere a reflective surface forms as part of the interannual variability, whereas in the Southern Hemisphere a reflective surface forms each year as part of the seasonal cycle.

Table 1 also shows that U and \bar{q}_y are significantly positively correlated with m^2 . This is consistent with our finding that U is highly correlated with U_{zz} (-0.9) but not with U_z (0.25) for this period and region, and it suggests that the vertical wind curvature term is dominant in driving the interannual variability in \bar{q}_y . Figure 3 shows the yearly values of the averaged N^2 and U_{zz} . We see that N^2 shows a significant negative trend, while U_{zz} shows no significant trend (if anything, it is a small negative trend). This suggests that although the interannual variability in m^2 stems from changes in N^2 and U_{zz} , only the former contributes to the observed trend. These results indicate that the observed decadal changes in m^2 can be explained by observed significant trends in the mean flow zonal wind and temperature structure.

Shaw et al. (2010) showed that the formation of a vertical reflecting surface is not sufficient for downward wave coupling because the waves can disperse in the meridional direction. Downward wave coupling occurs when there is a high-latitude meridional waveguide, which is bounded above by a reflecting surface. Figure 4 shows the meridional wavenumbers for the same periods of Fig. 2. The shading now indicates regions where the waves cannot propagate in the meridional direction. For all decades, we see a clear meridional waveguide (the unshaded contoured meridional propagation region between 40° and 60°S, which is bounded by the shaded regions). To visualize the meridional-vertical wave propagation geometry, we also plotted the vertical reflecting surface (solid thick line). We see that during the last two decades, the lower-stratospheric meridional waveguide is narrower (the evanescent region at 40°S and 100–30 hPa appears in the first decade and widens with time), and the vertical reflecting surface is lower so that it better covers the region where the waves propagate upward. Shaw et al. (2010) called this wave geometry configuration, in which the reflecting surface spans the meridional waveguide, a *bounded wave geometry*. Waves propagating vertically along the meridional waveguide region are reflected down and guided back to the troposphere, where they influence the planetary wave field. Shaw et al. (2010) also showed that the climatological meridional waveguide is much narrower during late winter and spring than it is during early winter. We find

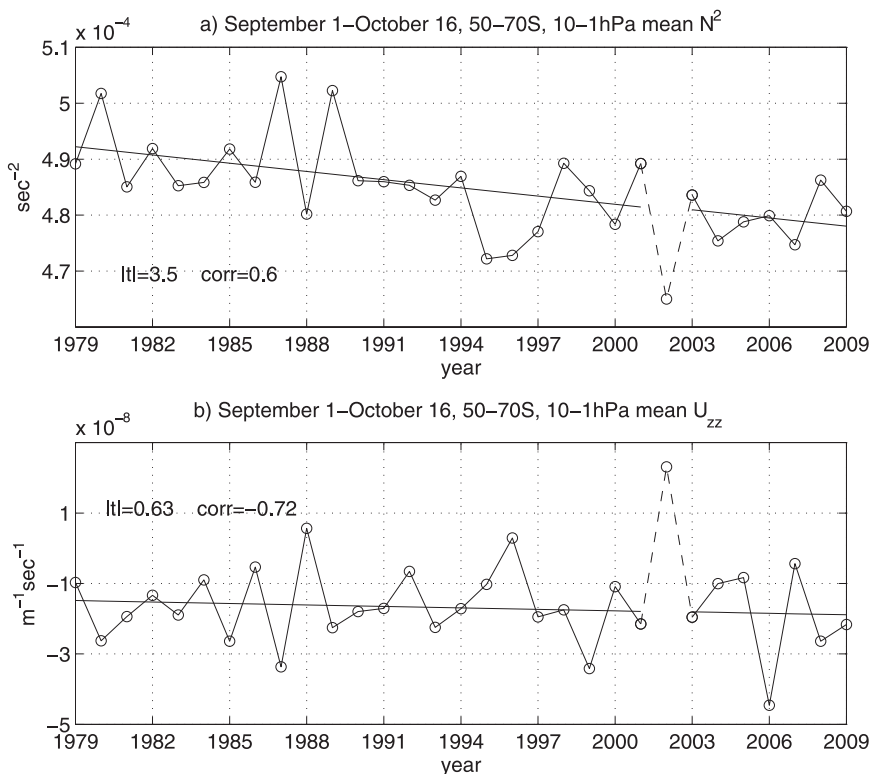


FIG. 3. Yearly values of the 1 Sep–16 Oct mean (a) Brunt Vaisalla frequency, and (b) vertical curvature of the zonal mean wind, averaged over 5–1 hPa and 50°–70°S (s^{-2} and $\text{m}^{-1} \text{s}^{-1}$, respectively), along with the linear best-fit regression. Sudden warming year 2002 is removed from the trend calculation.

that the transition to a narrower waveguide occurs earlier in the second two decades compared to the first (not shown). The yearly time series of the squared meridional wavenumber averaged from 100 to 30 hPa and 36°–46°S (representing the equatorward boundary of the waveguide; Fig. 4d) shows a clear negative trend, which is significant at the 97% level based on a single-sided t test ($|t| = 2.01$). The combined changes in vertical and meridional wavenumbers are consistent with the increase in the September–October downward wave cross correlations shown in Fig. 1. While the bounded wave geometry, which is favorable for downward wave coupling, starts in early October during the 1970s, it starts in September during the 1980s and 1990s.

We next turn to examine the observed changes in downward wave coupling during November–December. Previous studies have shown that the breakup of the polar vortex has been delayed in recent decades (e.g., Neff 1999; Waugh et al. 1999; Black and McDaniel 2007). This has been attributed to ozone depletion (e.g., Haigh and Roscoe 2009). We expect this delay in the vortex breakup to allow upward wave propagation and downward wave reflection to last longer into December, and therefore it can be used to explain the observed

increase in upward and downward wave coupling during November–December (bottom row of Fig. 1). To identify the vortex breakup, we calculate the midstratospheric (30–10 hPa) zonal-mean zonal wind ($\langle U(30-10) \rangle$) and define the vortex breakup date as the day on which the 55°–75°S mean $\langle U(30-10) \rangle$ first becomes negative during November–December. The vortex breakup day, counted from 1 January, is denoted by df and plotted in Fig. 5. There is a lot of variability in the vortex breakup date; however, there is a discernible positive trend.² The largest and most significant trend occurs from 1979 to 1999 (thick straight line) and is statistically significant at the 98.8% level based on a one-sided t test ($|t| = 2.42$), while the trend over the entire period (thin straight line) is only significant at the 88% level ($|t| = 1.16$). If the sudden warming year 2002 is removed, then the trend over the entire period is significant at the

² The nature of both the interannual variability and trend of the vortex breakup is consistent with the timing of the initial spring increases in the stability in the layer from 150 to 100 hPa, based on rawinsonde data for the period from 1979 to 1998 Neff (1999) and its update to 2009 (B. Neff 2010, personal communication).

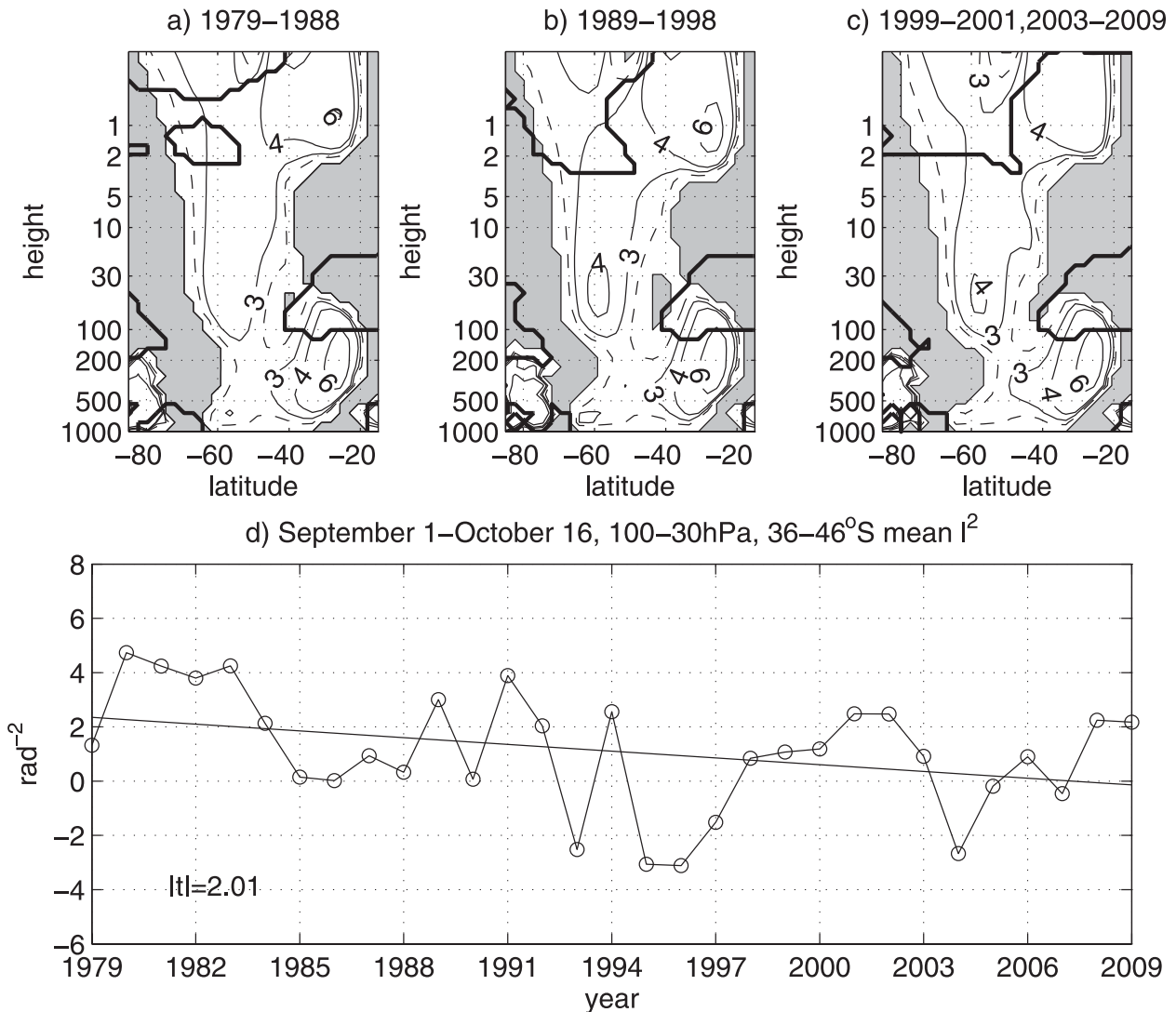


FIG. 4. Decadal meridional wavenumbers for 1 Sep–16 Oct for (a) 1979–88, (b) 1989–99, and (c) 1999–2009, excluding 2002. Evanescent regions (negative l^2) are shaded. Contour values, in units of rad^{-1} , are 2 (dashed), and 3, 4, and 6 (solid). Also shown is the vertical reflecting surface (thick solid lines) from Fig. 2. (d) Yearly values and linear best-fit regression (straight lines) of the 1 Sep–16 Oct mean meridional wavenumber squared, averaged over 100–30 hPa and 36° – 45° S (units of rad^{-2}).

97.1% level ($|t| = 1.97$). The smaller trend significance for the longer period is consistent with the saturation of ozone depletion observed since the late 1990 (Langematz and Kunze 2006). However, the leveling off of the trend may also be associated with increased wave activity, which would lead to an earlier breakup date (e.g., Hu and Fu 2009; Akiyoshi et al. 2009).

To understand the effect of the delay in the vortex breakup date on the wave geometry, we calculate, for each year, the vertical and meridional wavenumbers during 20-day periods before and after the vortex breakup [i.e., $m(df - 25; df - 5)$, $l(df + 5; df + 25)$], with the averaging period taken up to 31 December for all

years] and then average over all years. Figures 6a,b show the post- and prevortex breakup wave geometries. Before the vortex breakup, vertical wave propagation can occur up to about 10 hPa and there is a well-defined high-latitude meridional waveguide in the lower stratosphere (between 100 and 30 hPa; Fig. 6a). This is a characteristic spring wave geometry. After the vortex breakup, the wave geometry is more characteristic of a summer stratospheric basic state, with the higher-latitude stratospheric waveguide essentially disappearing by shifting equatorward to where the vertical propagation is blocked above 100 hPa (Fig. 6b). This equatorward shift of the waveguide is consistent with the observations

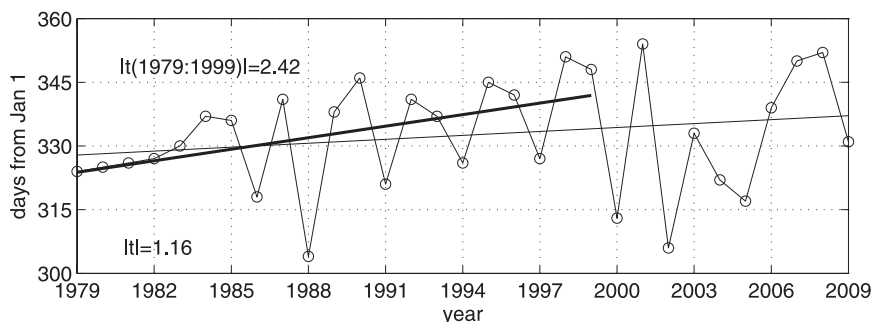


FIG. 5. Yearly time series (circled line) with the linear trends and $|t|$ values based on 1979–2009 (excluding the September 2002 sudden warming) and 1979–99 (thin and thick straight lines, respectively) of the day on which the zonal-mean wind, averaged over 30–10 hPa and 54°–75°S, first becomes zero, counting from 1 Jan.

of Black and McDaniel (2007), who showed that Southern Hemisphere final warmings organize the tropospheric circulation during the period following the warming, with high-latitude deceleration and low-latitude acceleration of the upper-tropospheric zonal mean wind. We note that Black and McDaniel (2007) also found zonally asymmetric anomalies in the lower troposphere associated with the vortex final warming, which could be related to the above changes in downward wave reflection.

Given the delay in the vortex breakup date from sometime in November during the 1980s to sometime in December during the 1990s and 2000s, the November–December mean vortex state will be more like the post-breakup state (Fig. 6b) in the 1980s and more like the prebreakup state (Fig. 6a) in the 1990s and 2000s. To examine this in more detail, we calculate the yearly time series of the 31 October–20 December mean m and l from [chosen to include all the vortex breakup dates: $\min(df) - 5$; $\max(df) + 5$]. Figure 6c shows the yearly time series of m^2 averaged between 55 and 15 hPa and 50°–70°S. This averaging region captures the waveguide itself, so that m^2 averaged over this area will be positive before the vortex breakup (when we have significant downward wave coupling) and negative after the vortex breakup (when there is no more stratosphere–troposphere wave coupling in either vertical direction).³ The clear positive m^2 trend during the first two decades, followed by a highly variable third decade (Fig. 6c), is thus consistent with the November–December mean

wave geometry changing from a predominantly summer state of no stratosphere–troposphere wave coupling (Fig. 6b) in the 1980s to a prevortex breakup wave geometry (Fig. 6a) with significant downward wave coupling during the 1990s–2000s.

We also plot the meridional wavenumber squared averaged between 100 and 10 hPa and 40°–50°S. This averaging region lies just equatorward of the midwinter stratospheric waveguide, so that before the vortex breakup, l^2 is negative; however, after the vortex breakup, the upper tropospheric–lower stratospheric waveguide shifts equatorward, rendering this index positive. The observed negative trend in l^2 , shown in Fig. 6d, is again consistent with the observed delay in the vortex breakup and the increase in downward wave coupling.

Further examination of the interannual variability shows clear correlations between the averaged squared wavenumbers and the vortex breakup date time series. The correlations between the detrended df and the detrended $\langle m^2 \rangle$ and $\langle l^2 \rangle$ are 0.79 and -0.83 , respectively. The 1979–2009 and 1979–99 trends are shown (thin and thick straight lines, respectively) with the corresponding $|t|$ values stated on the plot in lightface and bold, respectively. As for df , the linear trends in m^2 and l^2 are significant at least at the 99% level during the first two decades, and there is a saturation in the third decade. Removing the year 2002 increases the significance of the 1979–2009 trend, especially for l^2 ($|t|$ values of 1.69 instead of 1.16 for df , 2.58 instead of 1.83 for m^2 , and 2.77 instead of 2.00 for l^2). The results clearly demonstrate that the delay in the vortex breakup date causes the bounded wave geometry to last longer, leading to enhanced downward wave reflection and hence larger downward wave coupling during November–December.

Figure 1 showed that the September–October and November–December correlations increased significantly with time, whereas the October–November correlations

³ We note that in Fig. 2d although we plotted m^2 in the region where the reflection surface formed (5–1hPa), whereas here we are showing m^2 in the middle of the vertically bounded waveguide (55–15hPa). Thus, a decrease in m^2 with time means more wave reflection in Fig. 2d, but less wave reflection and downward coupling in Fig. 6c.

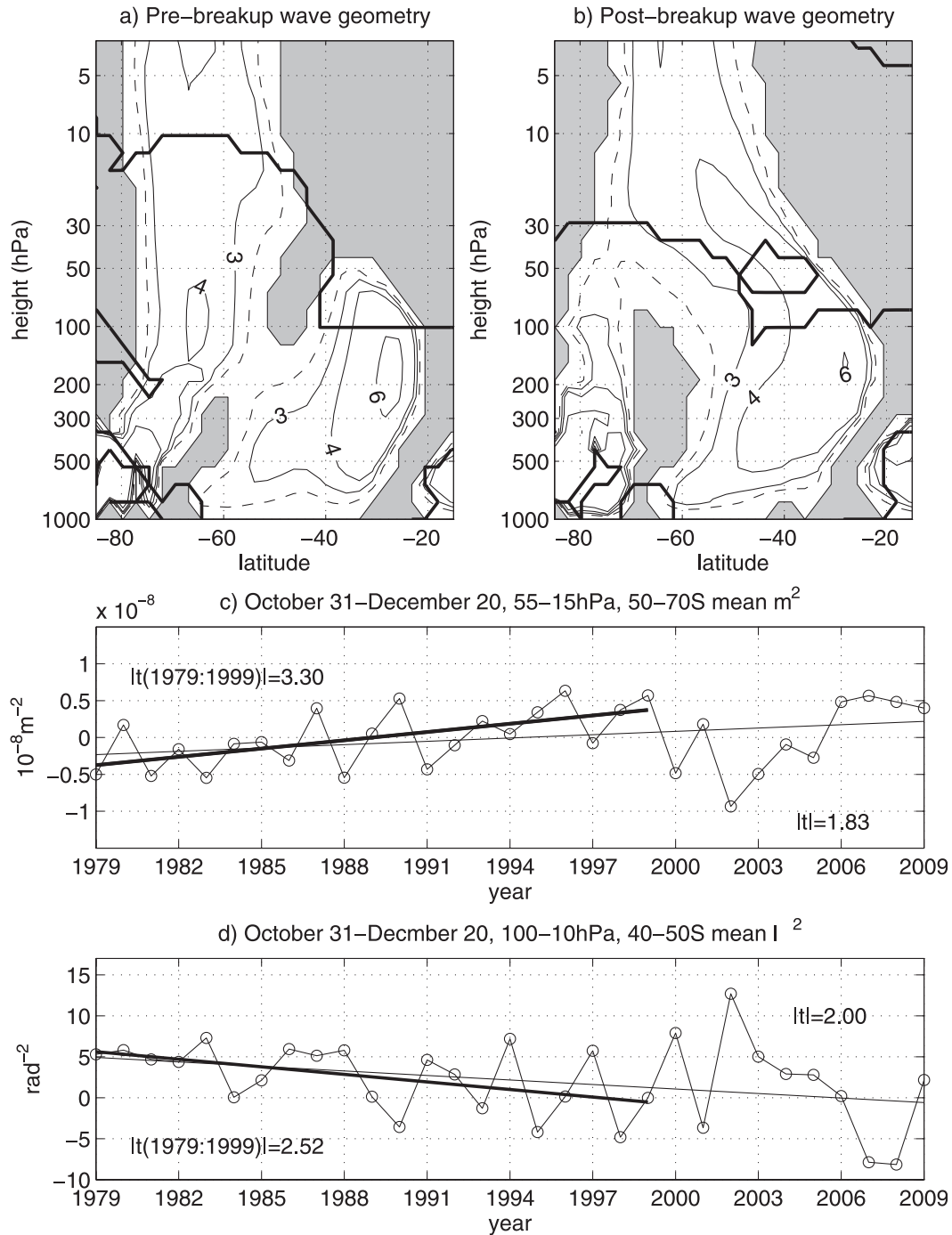


FIG. 6. The 1979–2009 mean meridional wavenumbers (thin contours) and vertical reflecting surface (thick contour) for the 20 days (a) before and (b) after the final warming date, defined by the index of Fig. 5. Contouring and shading in (a), (b) as in Figs. 4a–c. Yearly time series (circled line) with the linear trends based on 1979–2009 and 1979–99 (thin and thick straight lines, respectively) of the 31 Oct–20 Dec mean (c) vertical wavenumber squared averaged over 55–15 hPa and 50°–70°S (units of $10^{-8} m^{-2}$) and (d) meridional wavenumber squared, averaged over 100–10 hPa and 40°–50°S (units of rad^{-2}).

did not show significant trends. Consistently, we find that the wave geometry did not change significantly from 17 October to the vortex breakup date df (not shown). Thus, the main changes in downward wave coupling result from changes at the beginning and end of the wave reflective season. The combination of the earlier onset of the bounded wave geometry (from early October to September) and the vortex breakup shifting from late November to December causes the significant increase in the September–December downward wave coupling.

4. Summary and discussion

This paper examines the decadal changes in downward wave coupling using the MERRA reanalysis dataset from 1979 to 2009. Downward wave coupling is identified using cross-coherence correlations between stratospheric and tropospheric wave 1 geopotential height fields. The wave coupling is related to the basic state using wave geometry diagnostics for stationary zonal wave 1. We find a significant increase in downward wave coupling during the September–December period as well as during the September–October and November–December subperiods over the last three decades. The increase is related to a change in the timing of the bounded wave geometry configuration, which is favorable for downward wave coupling. The bounded wave geometry starts earlier in the season (early September) and lasts longer (into December) with little change in the middle of the reflective period (from mid-October to the vortex breakup date).

The causes of the observed decadal changes in the wave geometry, which result in changes in the downward wave coupling, have not been attributed so far and are only partially understood. Our analysis reveals that the extension of the bounded wave geometry into November–December is most likely caused by a delay in the vortex breakup, which has been linked to stratospheric ozone depletion (Haigh and Roscoe 2009). However, increases in planetary wave driving during winter and early spring, which have been observed in the 2000s, also affect the vortex persistence (Langematz and Kunze 2006). The changes in the wave geometry during September–October are clearly related to changes in the stratospheric vortex structure, particularly in the upper stratosphere in mid- and high latitudes; however, the contribution of stratospheric ozone changes, SST changes, and other processes to these mean flow changes is not clear. We note that during November–December, both the upward and downward wave correlations increased; however, in September–October, the upward wave correlations remain unchanged over the decades.

Because the trend calculations are based on a reanalysis product, we cannot preclude impacts of the changing observing system on the decadal changes, especially in the mid- to upper stratosphere. We also note that the meridional and vertical wavenumber calculations involve highly derived quantities that increase the uncertainties in their trend estimates. However, we found that the MERRA decadal changes in both the wave geometry and wave 1 cross correlations for the period 1979–98 were very close to those from ERA-40. Furthermore, the MERRA decadal cross-correlation changes during the period 1979–2009 agree well with similar estimates based on the National Centers for Environmental Prediction (NCEP)/Department of Energy (DOE) Atmospheric Model Intercomparison Project, phase 2 (AMIP-II) Reanalysis (R-2) (Kanamitsu et al. 2002). Overall, the wave 1 decadal cross correlations are more reliable because they are directly based on geopotential heights, which is a class A reanalysis field in the troposphere and lower stratosphere.⁴ The consistency of the two diagnostics (cross correlations and wave geometry) suggests that the changes in the wave geometry are also reliable and furthermore that the decadal changes in downward coupling are not an artifact of the changing observing system.

Atmospheric general circulation models can be used to assess the causes for the observed increase in downward wave coupling. However, the model must have a proper representation of the climatology of the stratospheric basic state and downward wave coupling (Shaw et al. 2010). In the companion paper Shaw et al. (2011), we use the Goddard Earth Observing System chemistry–climate model and attribute the increase of downward wave coupling in the model to ozone depletion. As in the November–December observations (we do not discuss September–October changes in this paper), the model shows an increase in downward cross correlations when forced with observed changes in halogens. These are related to ozone-induced changes in the wave geometry, which cause a delay in the vortex breakup date. When the model was run with fixed chlorine (so no ozone depletion evolved in the stratosphere), there was no significant change in the downward wave coupling.

Previous studies have emphasized the importance of changes in zonal-mean stratosphere–troposphere coupling since 1979 and their impact on the Southern Hemisphere annular mode [see Son et al. (2010), for an overview of identified mechanisms]. More recent studies

⁴ According to Kalnay et al. (1996), a reanalysis gridded field is classified as class A analysis variable when it is strongly influenced by observed data and hence most reliable.

have pointed out significant observed nonzonal decadal trends (Neff et al. 2008; Lin et al. 2009; Hu and Fu 2009). Our study shows that in addition to changes in zonal-mean coupling, there has been a significant change in downward wave coupling since 1979. Understanding to what degree changes in downward wave coupling explain the observed nonzonal decadal trends in the Southern Hemisphere is a work in progress.

Acknowledgments. NH was supported by Grant 1370/08 from the Israeli Science Foundation. JP acknowledges support from the NASA Modeling and Analysis program. TAS was supported by a postdoctoral fellowship from the Natural Sciences and Engineering Research Council of Canada. The authors thank Bill Neff and Steven Pawson for their helpful input and discussions. We thank two anonymous reviewers for their comments, which helped us clarify the manuscript.

REFERENCES

- Akiyoshi, H., and Coauthors, 2009: A CCM simulation of the breakup of the Antarctic polar vortex in the years 1980–2004 under the CCMVal scenarios. *J. Geophys. Res.*, **114**, D03103, doi:10.1029/2007JD009261.
- Black, R. X., and B. McDaniel, 2007: Interannual variability in the Southern Hemisphere circulation organized by stratospheric final warming events. *J. Atmos. Sci.*, **64**, 2968–2975.
- Gillett, N. P., and D. W. J. Thompson, 2003: Simulation of recent Southern Hemisphere climate change. *Science*, **302**, 273–275.
- Haigh, J. D., and H. K. Roscoe, 2009: The final warming date of the Antarctic polar vortex and influences on its interannual variability. *J. Climate*, **22**, 5809–5819.
- Harnik, N., 2009: Observed stratospheric downward reflection and its relation to upward pulses of wave activity. *J. Geophys. Res.*, **114**, D08120, doi:10.1029/2008JD010493.
- , and R. S. Lindzen, 2001: The effect of reflecting surfaces on the vertical structure and variability of stratospheric planetary waves. *J. Atmos. Sci.*, **58**, 2872–2894.
- Hu, Y., and Q. Fu, 2009: Stratospheric warming in Southern Hemisphere high latitudes since 1979. *Atmos. Chem. Phys.*, **9**, 4329–4340.
- Johanson, C. M., and Q. Fu, 2007: Antarctic atmospheric temperature trend patterns from satellite observations. *Geophys. Res. Lett.*, **34**, L12703, doi:10.1029/2006GL029108.
- Kalnay, E., and Coauthors, 1996: The NCEP/NCAR 40-Year Reanalysis Project. *Bull. Amer. Meteor. Soc.*, **77**, 437–471.
- Kanamitsu, M., W. Ebisuzaki, J. Woollen, S.-K. Yang, J. J. Hnilo, M. Fiorino, and G. L. Potter, 2002: NCEP–DOE AMIP-II Reanalysis (R-2). *Bull. Amer. Meteor. Soc.*, **83**, 1631–1643.
- Langematz, U., and M. Kunze, 2006: An update on dynamical changes in the Arctic and Antarctic stratospheric polar vortices. *Climate Dyn.*, **27**, 647–660, doi:10.1007/s00382-006-0156-2.
- Lau, K. M., and P. H. Chan, 1983: Short-term climate variability and atmospheric teleconnections from satellite-observed outgoing longwave radiation. Part II: Lagged correlations. *J. Atmos. Sci.*, **40**, 2751–2767.
- Lin, P., Q. Fu, S. Solomon, and J. W. Wallace, 2009: Temperature trend patterns in Southern Hemisphere high latitudes: Novel indicators of stratospheric change. *J. Climate*, **22**, 6325–6341.
- Neff, W., 1999: Decadal time scale trends and variability in the tropospheric circulation over the South Pole. *J. Geophys. Res.*, **104**, 27 217–27 251.
- , J. Perlwitz, and M. Hoerling, 2008: Observational evidence for asymmetric changes in tropospheric heights over Antarctica on decadal time scales. *Geophys. Res. Lett.*, **35**, L18703, doi:10.1029/2008GL035074.
- Perlwitz, J., and N. Harnik, 2003: Observational evidence of a stratospheric influence on the troposphere by planetary wave reflection. *J. Climate*, **16**, 3011–3026.
- , and —, 2004: Downward coupling between the stratosphere and troposphere: The relative roles of wave and zonal mean processes. *J. Climate*, **17**, 4902–4909.
- Randel, W. J., 1987: A study of planetary waves in the southern winter troposphere and stratosphere. Part I: Wave structure and vertical propagation. *J. Atmos. Sci.*, **44**, 917–935.
- , 1988: The seasonal evolution of planetary waves in the Southern Hemisphere stratosphere and troposphere. *Quart. J. Roy. Meteor. Soc.*, **114**, 1385–1409.
- Rienecker, M. M., and Coauthors, 2011: MERRA—NASA’s Modern-Era Retrospective Analysis for Research and Applications. *J. Climate*, **24**, 3624–3648.
- Schubert, S., and Coauthors, 2008: Assimilating earth system observations at NASA: MERRA and beyond. *Extended Abstracts, Third WCRP Int. Conf. on Reanalysis*, Tokyo, Japan, WCRP, V1-103. [Available online at http://wcrp.ipsl.jussieu.fr/Workshops/Reanalysis2008/Documents/V1-104_ea.pdf.]
- Shaw, T. A., J. Perlwitz, and N. Harnik, 2010: Downward wave coupling between the stratosphere and troposphere: The importance of meridional wave guiding and comparison with zonal-mean coupling. *J. Climate*, **23**, 6365–6381.
- , —, —, P. A. Newman, and S. Pawson, 2011: The impact of stratospheric ozone changes on downward wave coupling in the Southern Hemisphere. *J. Climate*, **24**, 4210–4229.
- Son, S.-W., and Coauthors, 2010: Impact of stratospheric ozone on Southern Hemisphere circulation change: A multimodel assessment. *J. Geophys. Res.*, **115**, D00M07, doi:10.1029/2010JD014271.
- Thompson, D. W. J., and S. Solomon, 2002: Interpretation of recent Southern Hemisphere climate change. *Science*, **296**, 895–899.
- Waugh, D., W. Randel, S. Pawson, P. Newman, and E. Nash, 1999: Persistence of the lower stratospheric polar vortices. *J. Geophys. Res.*, **104**, 27 191–27 201.